MIT Libraries | DSpace@MIT

MIT Open Access Articles

Molecular Modeling and Mechanics of Acrylic Adhesives on a Graphene Substrate with Roughness

The MIT Faculty has made this article openly available. ***Please share*** how this access benefits you. Your story matters.

Citation: Qin, Zhao, Kai Jin, and Markus J. Buehler. "Molecular Modeling and Mechanics of Acrylic Adhesives on a Graphene Substrate with Roughness." BioNanoScience 6, no. 3 (June 9, 2016): 177–184.

As Published: http://dx.doi.org/10.1007/s12668-016-0205-1

Publisher: Springer US

Persistent URL: http://hdl.handle.net/1721.1/107452

Version: Author's final manuscript: final author's manuscript post peer review, without publisher's formatting or copy editing

Terms of use: Creative Commons Attribution-Noncommercial-Share Alike

Massachusetts Institute of Technology

BioNanoSci. (2016) 6:177–184
DOI 10.1007/s12668-016-0205-1

Molecular Modeling and Mechanics of Acrylic Adhesives on a Graphene Substrate with Roughness

Zhao Qin[1] · **Kai Jin**[1] · **Markus J. Buehler**[1]

Published online: 9 June 2016
© Springer Science+Business Media New York 2016

Abstract Understanding the mechanics of amorphous polymeric adhesives on a solid substrate at the fundamental scale level is critical for designing and optimizing the mechanics of composite materials. Using molecular dynamics simulations, we investigate the interfacial strength between graphene and polyacrylic and discuss how the surface roughness of graphene affects the interfacial strength in different loading directions. Our results show that a single angstrom increase in graphene roughness can lead to almost eight times higher shear strength, and that such result is insensitive to compression. We have also revealed that the graphene roughness has modest effect on tensile strength of the interface. Our simulations elucidate the molecular mechanism of these different effects in different loading conditions and provide insights for composite designs.

Keywords Mechanics · Adhesion · Strength · Molecular dynamics

1 Introduction

The mechanics of amorphous polymeric adhesives on a solid substrate is critical for interfacial interaction for both natural and synthetic composite materials [1–8]. In nature, they are often found in the forms of biological polymers, such as protein, chitin, and glucose, and they play an important role to integrate different materials of contrasting mechanical or chemical properties, allowing these material building blocks to synergistically assemble and form new composite materials with mechanical functions superior to each of their building blocks [3, 6–8]. For example, the shell of nacre is mainly composed of the assembly of polygonal mineral tablets with hundreds of nanometers in thickness that are made of calcium carbonate, and they bind with each other on the contact surface by organic polymeric materials [1]. Molecular nonbonded interactions including van der Walls forces, hydrogen bonding, and electrostatic interactions play the dominating role for adhesion, and it is fascinating that these relatively weak interactions can integrate the mineral tablets to achieve both outstanding stiffness and toughness at the same time, which is usually a drawback for many engineering materials [9]. Learning the molecular deformation mechanisms of adhesives at their interface with solid substrates will be beneficial to generate knowledge and insights that could be helpful to design and tailor the mechanical functions of composite materials.

Graphene as one of the two-dimensional materials that were discovered in recent years has several material advantages for making synthetic composites [10, 11]. It is the strongest and stiffest material known so far. Moreover, it is of only single-atom thickness, of good thermal and electrical conductivity, as well as optically transparent. Graphene is naturally discovered in the form of graphite, which is known to have a weak interlayer interaction, and one cannot expect to produce a reliable composite by simply stacking them together [12]. Chemical methods including functionalizing the graphene by decorating chemical groups on the graphene surface can enhance the interfacial interaction by forming covalent bonds but will simultaneously change its mechanical and chemical

✉ Markus J. Buehler
mbuehler@MIT.EDU

[1] Laboratory for Atomistic and Molecular Mechanics (LAMM), Department of Civil and Environmental Engineering, Massachusetts Institute of Technology, 77 Massachusetts Ave., Cambridge, MA, USA

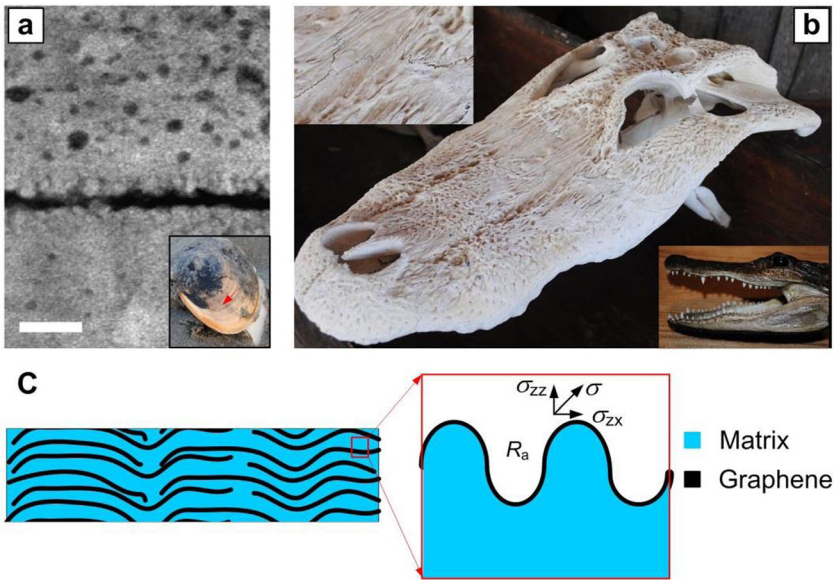

Fig. 1 Image of examples of biological materials and schematic of bio-inspired composite based on graphene and polymer matrix. **a**. Nacre and its microscopic structure at the rough interface between two neighboring mineral layers, which are buffered by an organic layer of ~8 nm in thickness, *Scale bars*, 50 nm (image reproduced from [1] under a Creative Commons Attribution 4.0 International License). *Insert*: photo of a clam (credits to Z.Q.). **b**. A crocodile skull shows an interface between two neighboring pieces of the bone with a clear zig-zag pattern (photos credit to Z.Q.). **c**. A schematic of a composite material based on graphene and polymer matrix with their interfaces defined by the surface roughness of graphene (R_a). The loading stress on the interface can be separated into shear stress and tensile stress

property [13]. Referring to natural systems such as nacre interface and suture of the bone as shown in Fig. 1a, b, respectively, covalent bonds are rarely used but the structure of the interface plays an important role in governing the interfacial mechanics [1, 7, 14]. Graphene is known to be extremely flexible, and a small mechanical fluctuation can lead to non-zero roughness because of its out-of-plane deformation such as wrinkle and crumple. It is interesting to ask how the adhesion force between polymeric adhesive and graphene will change with its roughness, as schematically shown in Fig. 1c, which may be useful for both adhesive and composite designs.

Molecular dynamics is an effective tool that has proven extremely useful in elucidating molecular mechanics of polymer materials and its adhesion to other inorganic substrates at the extremely small length scales which currently are not accessible with experimental techniques [4]. Such models have successfully been used to investigate a broad range of polymer systems including basic dynamics and structure of amorphous polymers [15, 16], adhesion of end-tethered polymers [17, 18], and properties of highly crosslinked network polymer adhesives [19–22]. Here, we use a simple full atomic molecular dynamics model to directly investigate the extent to which the surface roughness of graphene can affect the adhesion force with a polyacrylic (PA) adhesive. We provide quantitative insights into how the mechanics of adhesive and interfacial structure can synergistically contribute to the interfacial adhesion with graphene which can be used to tune and optimize the adhesive performance and mechanics of graphene-based composites.

2 Model and Methods

2.1 Atomistic Polyacrylic Model for Simulations

We employ a simple full atomic model of PA based on the assembly of 60 polymer chains with each of them composed of 30 PA acids with a chemical formula as $(C_3H_4O_2)_{30}$ as shown in Fig. 2a. A flat sheet of graphene without roughness is modeled by a planar hexagonal lattice with a lattice constant of 1.41 Å. This PA chains are initially randomly oriented with at least 40 Å away from the top surface of graphene. The interactions among atoms of PA chains and graphene are described by the consistent valence force field (CVFF) [23], which is a generalized valence force field with parameters provided for amino acids, water, and a variety of other functional groups.

$$E = \sum E_{\text{bond}} + \sum E_{\text{nonbond}} \quad (1)$$

Equation (1) generally represents the total energy (E) of the system that is composed of E_{bond} as the sum of interactions via covalent bonds which is composed of deformation energy of bond lengths, bond angles, torsion angles, and out-of-plane interactions, respectively, as well as E_{nonbond} as the sum of

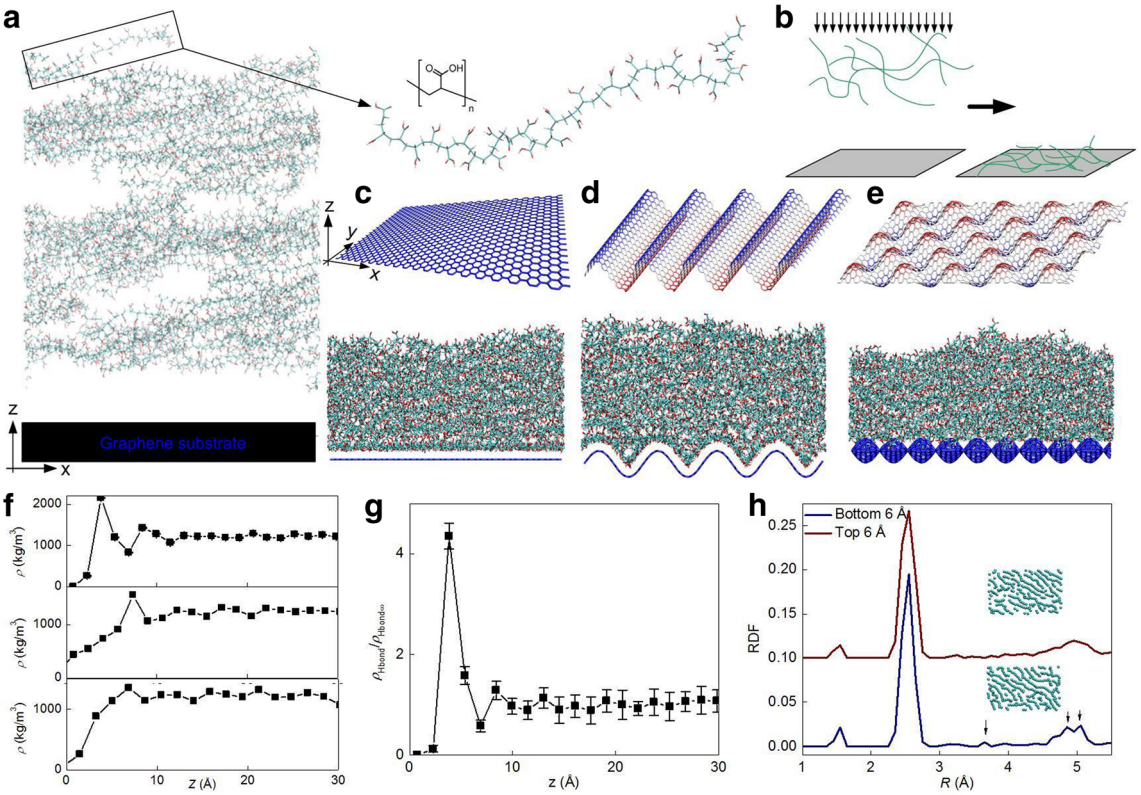

Fig. 2 Preparation and structure feature of the graphene-PA interface. **a**. The initial conformation of the simulation system with graphene substrate and randomly oriented PA polymer chains with at least 40 Å away from the top surface of graphene. Each chain is composed of 30 PA acids. **b**. The schematic of the equilibrium process of the simulation system as the polymer chains subjected to gravity force get deposited toward the graphene substrate. **c**–**e**. Graphene of different geometry and roughness is used in this study, which largely determines the equilibrated geometry of the polymer material at the interface, as shown by the simulation snapshots, and these models have roughness of 0, 2.3, and 1.5 Å, respectively. **f**. The distributions of the density (ρ) of PA at the interface as a function of its distance from the graphene surface for different surfaces as shown in panels **c**, **d**, and **e**, respectively. **g**. The distribution of the density (ρ_{Hbond}) of hydrogen bonds at the interface as a function of its distance from the graphene surface. This value is normalized by the bulk state density value ($\rho_{\mathrm{Hbond}\infty}$) as what is measured at the place far from the substrate surface. **h**. The radial distribution functions (RDF) of the carbon atoms of a layer of polymer chains with 6 Å in thickness at the bottom of the simulation system (*blue curve*) and that at the top of the simulation system (*red curve*). The *red curve* is shifted by 0.1 to get separated from the other curve. Two simulation snapshots of the carbon atoms in these two layers are inserted

the van der Waals interactions with a Lennard-Jones function and the Coulombic electrostatic interactions [23]. The model is implemented in the LAMMPS simulation package [24]. The simulation time step is 1 fs. Each simulation is performed in the NVT ensemble (constant temperature of 300 K and constant volume of the simulation system with the periodic boundary condition) in the purpose of getting an equilibrated structure with converged potential energy. Periodic boundary conditions are applied to all directions with a system size of $90 \times 50 \times 170$ Å^3. The nearest distance between two imaging models (30 Å) along the z direction is set to be far beyond the cutoff distance of van der Waals interactions as 10 Å, and the entire system has zero net charge, and thus, there is no interaction cross the periodic boundary in z direction. We use Ewald summation with relative error criterion of 10^{-4} to calculate the electronic interaction as an efficient method to accurately include all the long-distance electrostatics interactions. Visualizations of atomic structures are performed with VMD [25].

2.2 Assessment and Creation of Surface Roughness of Graphene

Considering that the most widely used one-dimensional roughness parameter is arithmetic average of absolute height values, the geometry of graphene in our system is characterized for its roughness with a definition as

$$R_a = \frac{1}{n}\sum_{i=1}^{n}\left|z_i - \frac{\sum_{i=1}^{n} z_i}{n}\right|, \tag{2}$$

where n is the amount of carbon atoms in graphene and z_i is the z coordinate of the atom i. To create a graphene substrate with desired roughness, we simply adopt a sinusoidal function as the targeting geometry. Such targeting geometry has its general function as

$$z_{i\_\mathrm{target}} = H\sin\left(2\pi x_i \,/\, L_x\right)\cos\left(2\pi y_i \,/\, L_y\right), \tag{3}$$

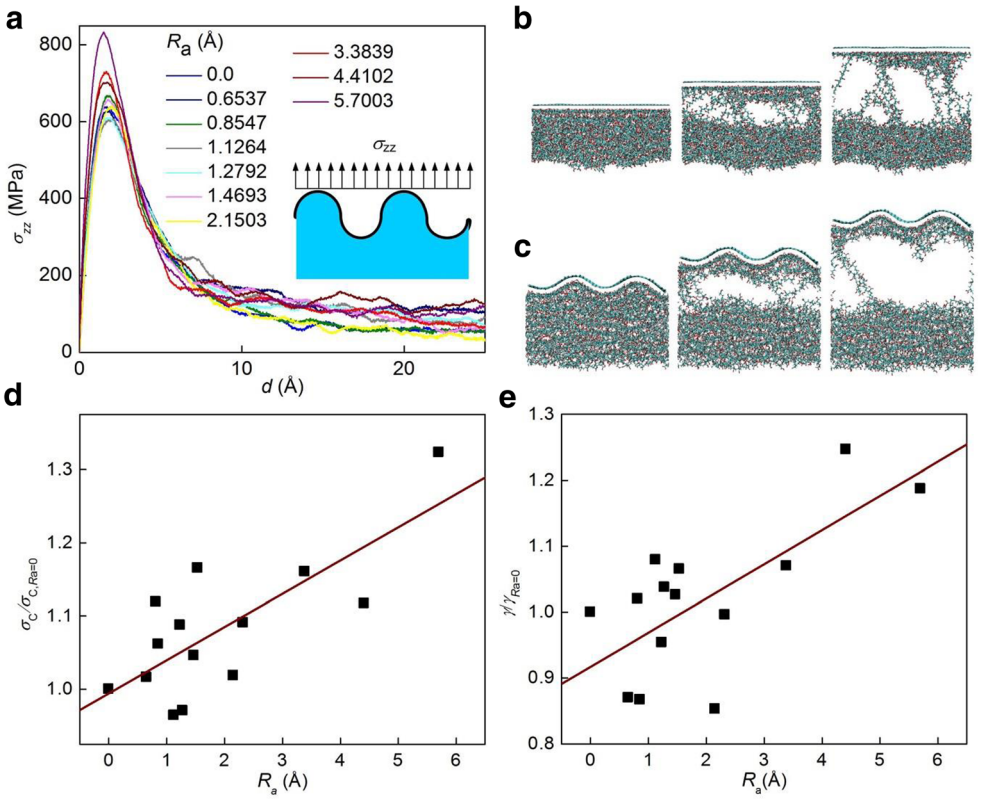

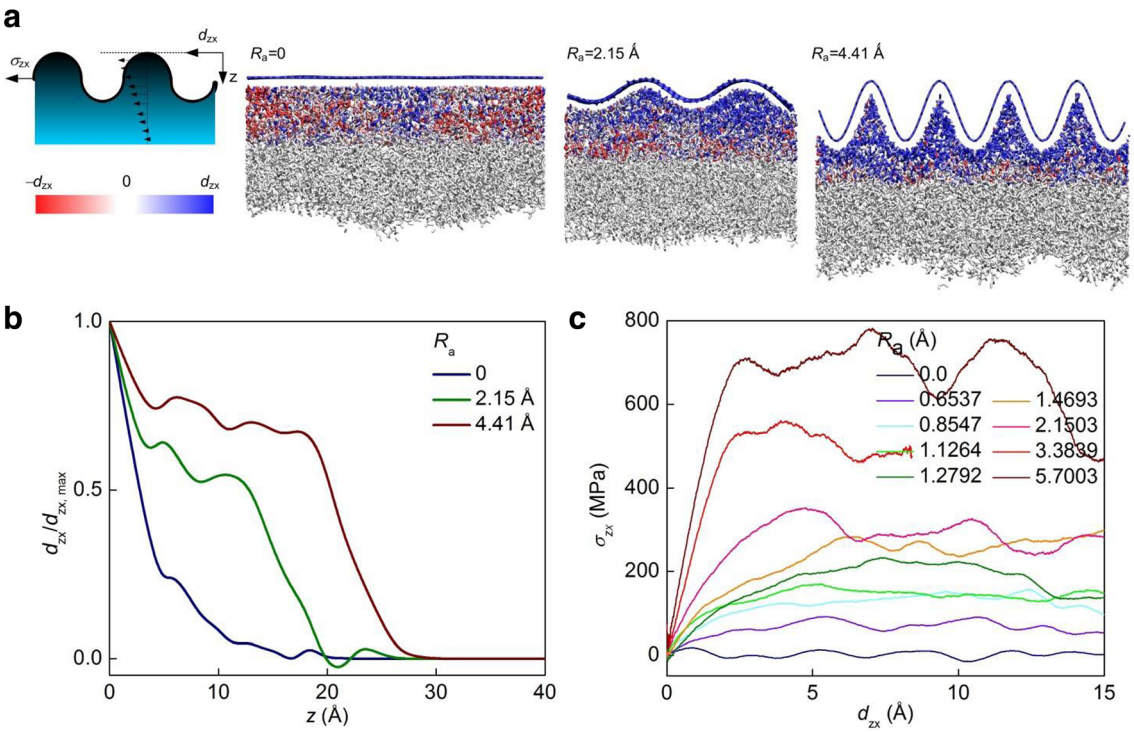

Fig. 3 The mechanical response of the graphene-PA interface that is subjected to tensile stress. **a**. The tensile-stress-displacement curves of different graphene-PA interfaces of graphene with different roughness. **b**–**c**. Simulation snapshots of different graphene-PA interfaces ($R_a = 0$ for **b** and 2.15 Å for **c**) with different displacement ($d = 0$, 20 and 40 Å from left to right). **d**. The peak tensile stress measured as a function of the surface roughness of the graphene. **e**. The toughness of the interface as a function of the surface roughness of the graphene. Data points in **d** and **e** are normalized by the case with $R_a = 0$, and their linear fits are given by the *solid curves*

Fig. 4 The mechanical response of the graphene-PA interface that is subjected to shear stress. **a**. Schematic of the loading condition and simulation snapshots for the examples with $R_a = 0$, 2.15, and 4.41 Å. Each atom is colored according to its displacement relative to the displacement of the graphene substrate under loading. **b**. The distribution of the averaged displacement of PA as a function of its distance from the top place of the graphene along the *z* axis. **c**. The shear-stress-displacement curves of different graphene-PA interfaces of graphene with different roughness

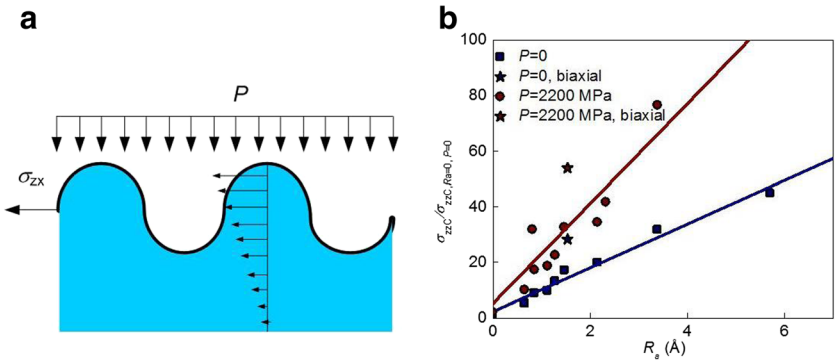

Fig. 5 The shear strength of the graphene-PA interface and its insensitivity to normal compression stress. **a**. Schematic of the loading condition with graphene subjected to both normal compression stress and shear deformation. **b**. Summary of the simulation results for the shear strength (σ_{zxc}) of graphene with different roughness (R_a) and that are subjected to different compression stress (P). Linear fits are made for the case $P = 0$ (details shown in Fig. 4) and $P = 2200$ MPa. σ_{zxc} for the graphene with a 2D wavy geometry (as shown in Fig. 2e) is given individually by *stars* to get distinguished from the 1D cases

where x_i and y_i are the x and y coordinates of each atom i, L_x and L_y are the period lengths in x and y directions, and H is the amplitude of the wave. For planar graphene, we use $H = 0$. For wavy graphene in one direction, we use $L_y = \infty$ and thus $\cos(2\pi y_i/L_y) = 1$ as the example geometry shown in Fig. 2d. For wavy graphene in the two directions, the example geometry is given as shown in Fig. 2e. Using the definition of roughness given in Eq. (2) and by assuming the atomic area is constant for carbon atoms, the roughness of the sinusoidal surface can be computed via $R_a = \frac{4}{L_x}\int_0^{\frac{L_x}{4}} z_{i\_target}dx = 2H / \pi$ for the 1D case and $R_a = \frac{16}{L_xL_y}\int_0^{\frac{L_y}{4}}\int_0^{\frac{L_x}{4}} z_{i\_target}dxdy = 4H / \pi^2$ for the 2D case. It is noted that for the same H value, the 2D case has a smaller roughness with a factor of $2/\pi$ than that of the 1D case.

A direct coordinate transformation from planar graphene to this geometry will generate a lot of residue stress in graphene, and thus, we execute a Monte Carlo (MC) simulation to get rid of the residue stress in graphene. To achieve that relaxation, we modify the total energy of graphene to be

$$E_{\text{graphene}} = \sum E_{\text{bond}} + \lambda\left(z_i - z_{i\_\text{target}}\right)^2 \quad (4)$$

where $\lambda = 100$ kcal/mol/Å^2 is a Lagrange multiplier for the constraint energy of the desired geometry. For each MC step, we randomly selected a single carbon atom and make a random movement trial. This trial leads graphene to a new potential energy state $E_{\text{graphene\_}t}$ from its old state of potential energy $E_{\text{graphene\_}0}$. The Metropolis criterion is used to decide whether or not to keep the movement or instead revert back to the old configuration with the acceptance probability as

$$P_{\text{accept}} = \min\left\{\exp\left(-\frac{E_{\text{graphene\_}t} - E_{\text{graphene\_}0}}{B}\right), 1\right\}, \quad (5)$$

where $B = 0.01$ kcal/mol is used here as an empirical parameter to accelerate the convergence of the total energy. We repeat this MC process for 500,000 steps to make sure to find the equilibrated graphene of different desired geometry as shown in Fig. 2c–e. This MC process is run by Matlab with own codes. It is noted that the graphene with a specific geometry is set to be rigid during following MD simulations in order to maintain its geometry through the PA deposition and loading tests. It is noted that several assumptions are made to the current study based on our full atomic model: 1. we do not consider the effects of defects and functional groups in the current study, and these effects have been addressed in the former studies [26–28]. Briefly, the randomly distributed vacancy can homogeneously weaken the interfacial interaction by decreasing the effective amount of contact surface area while such effect will not be strong for defects in the form of dislocations such as 5-7-7-5 or grain boundaries as the atomic area will not significantly change for these defect forms even with out-of-plane wrinkles [26]. Functional groups such as carboxyl and hydroxyl groups can homogeneously enhance the interfacial energy [27, 28]. 2. We only consider the uniform roughness in the study as the scale we are focusing on is relatively small. For modeling contact surface with a full-length scale, there will probably be heterogeneous roughness distribution but the problem will be more efficiently solved by mesoscopic models in the future studies. 3. We are considering that the graphene is interacting with a rigid substrate that is much stiffer than polymer on the other side. To simplify the simulation system and only focus on the effect of roughness on adhesion, we model the entire graphene as a rigid surface to keep its roughness a constant value during the simulation.

2.3 Gravity Force for Deposition Simulation

We fully equilibrate the systems in MD simulations to allow the initially randomly distributed PA chains to get freely deposited on graphene surface. Gravity force with acceleration of 10^{-4} Kcal/Å/g toward the $-z$ direction is

applied to all the PA atoms in the system in order to accelerate the deposition and assembly of PA chains. After 5 ns of MD simulation, we find the potential energy converges, and all the PA chains get deposited on graphene surface by adapting to its wavy geometry as shown in Fig. 2c–e. After that, we remove the gravity field and fully relax the system before performing loading tests.

2.4 Boundary Conditions of Graphene-PA Interface in Loading

For loading MD simulations, we set graphene as a rigid body and fix all the atoms of PA chains that are more than 20 Å from the mean z coordinate of the graphene. The graphene is moved with a constant velocity of 0.0001 Å/fs in either z axis (tensile as schematic in Fig. 3a) or x axis (shear as schematic in Fig. 4a). The total reaction force and displacement of the graphene are recorded during the test for post analysis.

3 Results and Discussion

We find that the PA deposited on graphene surface has a unique structure that is very different from its bulk state. The equilibrated graphene-PA system, as shown in Fig. 2c–e, shows an empty layer of space, which is caused by the van der Waals radius of graphene, followed by a much denser layer of PA material at its interface with graphene. This observation is quantified by the density distribution of PA materials on the planar graphene as shown in Fig. 2f, which shows that the PA has a much more varying density value within 15 Å from its interface with graphene. For the case with planar substrate, the two peak values at 3.8 and 8.4 Å from the graphene surface correspond to the center of two dense layers with higher mass density as 180 and 120 % of its bulk state. In comparison, the wrinkled geometries affect the density distribution at the interface by causing the layered structure (closest to graphene surface) to be mixed with the near-bulk state (far from graphene surface but still within the gap) at a same height from the bottom of the system. Although the peaks get less obvious for the wrinkled cases, there are still layered structures at the interface as can be seen in Fig. 2d. Moreover, such layered structure of contrasting density also corresponds to larger density of hydrogen bonds (H bonds) (Fig. 2g), as the first density peak corresponds to an H bond density that is more than four times than that of its bulk state. The singularity of mass and H bond distributions agrees with what has been observed for water at the interfaces with other nanomaterials [29–32]. In previous studies, it has been shown that a graphene substrate can lead to crystallization of polymer at the interface [33, 34] and thus yields enhanced mechanics at the interface [35]. Here, we compute the radial distribution function (RDF) of the carbon atoms of the polymer chains and compare its result for the bottom and the top polymers as shown in Fig. 2h. It is noted that the bottom chains show slightly more organized structure than the top chains but such a difference is not very significant as is probably limited by the small size of our simulation model. These evidences point to the fact that the mechanics of graphene-PA interface can be very different from its bulk state and thus is worth looking into by deforming the interface.

The results of tensile tests of the graphene-PA interface are summarized in Fig. 3. With the loading condition schematically shown in Fig. 3a, each stress-displacement curve corresponds to the mechanical response of a graphene-PA interface with a specific graphene roughness value. All of the structures initially feature a similar elastic response, followed by a peak stress (σ_c) and then a drop in the stress which corresponds to the formation of defects and rupture in the material, which is shown by the simulation snapshots in Fig. 3b. The long regime of plastic deformation after the stress peak corresponds to the sliding of polymer chains against each other in loading. The peak stress of each stress-displacement curve of specific surface roughness of graphene is summarized in Fig. 3c with all values normalized by the peak stress of the case of a planar graphene $\left(\sigma_{c,R_a}=0\right)$. As expected, the peak stress increases with increasing roughness due to the extra contact surface area between the graphene and the PA. However, the increase is modest—1-Å increment in R_a, which corresponds to a ~20 % more surface area than its projecting area, corresponds to only 4.5 % increase in σ_c. This statement is the same for both one-directional wavy graphene and two-directional wavy graphene. Moreover, such R_a insensitivity is similar for the toughness (γ) of the interface as summarized in Fig. 3d, which corresponds to the cumulative area below the stress-displacement curve, as 1-Å increment in R_a only leads to

Table 1 Summary of the main findings of the study

Loading Methods	Increment	Results In
Tensile	$R_a = 1$ Å	~4.5 % increment in strength, ~6 % increment in toughness
Shear	$R_a = 1$ Å	~770 % increment in both strength and toughness
Shear (with compression)	$P = 1$ atm.	<1 % increment in both strength and toughness for graphene with different R_a

The effects of surface roughness on the strength of graphene-PA interface with different loading methods

6 % increase in γ. For all of the graphene-PA interfaces considered with different graphene roughness, higher R_a overall results in an increase in the peak stress and toughness compared to the planar graphene, but again the effect is small. The mechanism can be obtained from the simulation snapshots as shown in Fig. 3b as the failure of the current interface is mainly governed by the separation of the PA material beyond the closest interface with graphene, which will not significantly change with R_a of graphene. Further introduction of crosslinks in the PA material can tune the mechanics of PA, which has been shown in our former study [4], and thus may enhance the effect of roughness on tensile strength and modulus.

The results of shear tests of the graphene-PA interface are summarized in Fig. 4. The test method is schematically shown in Fig. 4a, which also contains the simulation snapshots of different slightly deformed interfaces of specific R_a values. Figure 4c provides the stress-displacement curve for the mechanical response of each graphene-PA interface with a specific R_a value. All of the structures initially feature a similar elastic response, followed by a yield stress (σ_{zxc}) and then a plateau region for the ideal plastic deformation of the material in shear deformation. Again, it is noted that the trend is not affected by whether the graphene takes one-directional wavy geometry or two-directional wavy geometry. It is shown that the surface roughness of graphene has a much stronger effect on the shear stress, as a 1-Å increment in R_a leads to 770 % increase in σ_{zxc}, as the linear fit shown in Fig. 5b. The mechanism of this strong effect can be understood by examining the deformation profile of the PA at the interface, which is shown in Fig. 4a, b for three different systems for comparison. It is shown that for the planar graphene, the shear deformation leads to a strong slip boundary between the graphene because of the atomic smoothness of the graphene, and thus, the top layer of PA has a much smaller displacement than the graphene, suggesting that the PA provides small resistance force to keep the graphene from moving. The evidence is given by Fig. 4a as the displacement of each PA atom in the shear direction is given by its appearing color. For graphene with a larger R_a value, the slip boundary becomes much less severe as the PA trapped between two graphene surface peaks helps to lock the polymer material to move with graphene and also to dissipate the force along the polymer chain, which is supported by Fig. 4b as much more PA materials are involved in deformation ($R_a > 0$) than the planar case ($R_a > 0$). Moreover, for graphene with a larger R_a, the smallest distance between the graphene and the fix boundary gets smaller as we keep the PA material amount and projecting area to be constant, which may also contributed to the shear strength. This argument is supported by comparing the shear strength of the polymer on a 1D wavy graphene and that on a 2D wavy graphene as shown in Fig. 5b; as for the 2D case, a higher shearing strength is obtained than that of the 1D case of a same roughness. Considering the fact that the 2D case needs to have a higher amplitude with a factor of $\pi/2$ to reach the same roughness as the 1D case (see "Assessment and Creation of Surface Roughness of Graphene" section for detailed analysis), our results show that not only the roughness value but also the amplitude of wavy geometry should be important to determine the adhesion strength.

Finally, we investigate how the compression stress can alter the shear strength of the interface by repeating the shear tests and applying a normal stress on the graphene as shown in Fig. 5a. We find that the normal stress has only modest effect on the shear strength, as even an extremely strong compression of 2200 MPa can only leads to 170 to 240 % increase in σ_{zxc}, as shown in Fig. 5b. This result suggests that for a fully immersed graphene surface in a polymer matrix, increase of pressure may not be sufficient for a stronger interfacial interaction in shear deformation.

4 Conclusion

We summarize the main results of our simulations in Table 1. It is shown that the surface roughness of graphene has very different effects on the interfacial strength with PA for different loading conditions. We find that the roughness has a strong effect on shear strength, as by keeping the projecting area and PA amount at a constant value, a single angstrom increase in roughness can lead to 7.7 times stronger shear strength. We reveal that such effect is two orders of magnitude larger than its effect on tensile strength, which is limited by the strength of the non-crosslinked PA chains.

It is noted that the roughness in this study is mainly controlled by the amplitude of the sinusoidal function of the surface geometry. Other factors including wavelength and shape may also alter the result, as well as the mechanics of the PA material, which is governed by its crosslinking state. To evaluate these factors, a full atomic PA model may not be sufficient as it limits the system size and time scales for simulations, and thereby, a mesoscopic model will be more efficient to carry out the following up study to investigate the effect of all these factors.

According to what has been revealed in our study, by creating a rough surface of more complex structural features at the nanoscopic scale level, we can expect to achieve a stronger interfacial interaction between graphene and polymer matrix in shear deformation. As what has been shown in nature such as interface in nacre between mineral plate and suture of the bone. For layered composite materials such as the brick-and-

mortar designs [3, 36], a stronger interface in shearing means larger resistance in deformation, as well as larger energy dissipation during rupture. Considering these effects in composite design will contribute to both strength and fracture toughness of the composite and may eventually lead innovative composites with improved mechanics.

Acknowledgments We acknowledge support from Henkel Corporation. We acknowledge fruitful discussions with Dr. C. Paul.

References

1. Hovden, R., Wolf, S. E., Holtz, M. E., Marin, F., Muller, D. A., Estroff, L. A. (2015). Nanoscale assembly processes revealed in the nacroprismatic transition zone of Pinna nobilis mollusc shells. *Nature Communications, 6*, 10097.
2. Qin, Z., & Buehler, M. J. (2013). Impact tolerance in mussel thread networks by heterogeneous material distribution. *Nature Communications, 4*, 2187.
3. Dimas, L. S., Bratzel, G. H., Eylon, I., Buehler, M. J. (2013). Tough composites inspired by mineralized natural materials: computation, 3D printing, and testing. *Advanced Functional Materials, 23*(36), 4629–38.
4. Solar, M., Qin, Z., Buehler, M. J. (2014). Molecular mechanics and performance of crosslinked amorphous polymer adhesives. *Journal of Materials Research, 29*(9), 1077–85.
5. Qin, Z., & Buehler, M. J. (2014). Molecular mechanics of mussel adhesion proteins. *Journal of the Mechanics and Physics of Solids, 62*, 19–30.
6. Petrone, L., Kumar, A., Sutanto, C. N., Patil, N. J., Kannan, S., Palaniappan, A., et al. (2015). Mussel adhesion is dictated by time-regulated secretion and molecular conformation of mussel adhesive proteins. *Nature Communications, 6*, 8737.
7. Li, Y. N., Ortiz, C., Boyce, M. C. (2013). A generalized mechanical model for suture interfaces of arbitrary geometry. *Journal of the Mechanics and Physics of Solids, 61*(4), 1144–67.
8. Yang, W., Sherman, V. R., Gludovatz, B., Mackey, M., Zimmermann, E. A., Chang, E. H., et al. (2014). Protective role of Arapaima gigas fish scales: structure and mechanical behavior. *Acta Biomaterialia, 10*(8), 3599–614.
9. Knowles, T. P. J., & Buehler, M. J. (2011). Nanomechanics of functional and pathological amyloid materials. *Nature Nanotechnology, 6*(8), 469–79.
10. Geim, A. K., & Kim, P. (2008). Carbon wonderland. *Scientific American, 298*(4), 90–7.
11. Lee, C., Wei, X. D., Kysar, J. W., Hone, J. (2008). Measurement of the elastic properties and intrinsic strength of monolayer graphene. *Science, 321*(5887), 385–8.
12. Sen, D., Novoselov, K. S., Reis, P. M., Buehler, M. J. (2010). Tearing graphene sheets from adhesive substrates produces tapered nanoribbons. *Small, 6*(10), 1108–16.
13. Compton, O. C., Cranford, S. W., Putz, K. W., An, Z., Brinson, L. C., Buehler, M. J., et al. (2012). Tuning the mechanical properties of graphene oxide paper and its associated polymer nanocomposites by controlling cooperative intersheet hydrogen bonding. *ACS Nano, 6*(3), 2008–19.
14. Qin, Z., Pugno, N. M., Buehler, M. J. (2014). Mechanics of fragmentation of crocodile skin and other thin films. *Scientific Reports, 4*, 4966.
15. Auhl, R., Everaers, R., Grest, G. S., Kremer, K., Plimpton, S. J. (2003). Equilibration of long chain polymer melts in computer simulations. *Journal of Chemical Physics, 119*(24), 12718–28.
16. Kremer, K., & Grest, G. S. (1990). Dynamics of entangled linear polymer melts—a molecular-dynamics simulation. *Journal of Chemical Physics, 92*(8), 5057–86.
17. Sides, S. W., Grest, G. S., Stevens, M. J., Plimpton, S. J. (2004). Effect of end-tethered polymers on surface adhesion of glassy polymers. *Journal of Polymer Science Polymer Physics, 42*(2), 199–208.
18. Sides, S. W., Grest, G. S., Stevens, M. J. K. (2002). Large-scale simulation of adhesion dynamics for end-grafted polymers. *Macromolecules, 35*(2), 566–73.
19. Stevens, M. J. (2001). Manipulating connectivity to control fracture in network polymer adhesives. *Macromolecules, 34*(5), 1411–5.
20. Stevens, M. J. (2001). Interfacial fracture between highly cross-linked polymer networks and a solid surface: effect of interfacial bond density. *Macromolecules, 34*(8), 2710–8.
21. Tsige, M., Lorenz, C. D., Stevens, M. J. (2004). Role of network connectivity on the mechanical properties of highly cross-linked polymers. *Macromolecules, 37*(22), 8466–72.
22. Tsige, M., & Stevens, M. J. (2004). Effect of cross-linker functionality on the adhesion of highly cross-linked polymer networks: a molecular dynamics study of epoxies. *Macromolecules, 37*(2), 630–7.
23. Dauberosguthorpe, P., Roberts, V. A., Osguthorpe, D. J., Wolff, J., Genest, M., Hagler, A. T. (1988). Structure and energetics of ligand-binding to proteins—Escherichia coli dihydrofolate reductase trimethoprim, a drug-receptor system. *Proteins-Structure Function and Genetics, 4*(1), 31–47.
24. Plimpton, S. (1995). Fast parallel algorithms for short-range molecular-dynamics. *Journal of Computational Physics, 117*(1), 1–19.
25. Humphrey, W., Dalke, A., Schulten, K. (1996). VMD: visual molecular dynamics. *Journal of Molecular Graphics and Modelling, 14*(1), 33–8.
26. Qin, Z., Taylor, M., Hwang, M., Bertoldi, K., Buehler, M. J. (2014). Effect of wrinkles on the surface area of graphene: toward the design of nanoelectronics. *Nano Letters, 14*(11), 6520–5.
27. Nair, A. K., Qin, Z., Buehler, M. J. (2012). Cooperative deformation of carboxyl groups in functionalized carbon nanotubes. *International Journal of Solids and Structures, 49*(18), 2418–23.
28. Qin, Z., & Buehler, M. (2012). Bioinspired design of functionalised graphene. *Molecular Simulation, 38*(8–9), 695–703.
29. Qin, Z., & Buehler, M. J. (2015). Nonlinear viscous water at nanoporous two-dimensional interfaces resists high-speed flow through cooperativity. *Nano Letters, 15*(6), 3939–44.
30. Koga, K., Tanaka, H., Zeng, X. C. (2000). First-order transition in confined water between high-density liquid and low-density amorphous phases. *Nature, 408*(6812), 564–7.
31. Nanok, T., Artrith, N., Pantu, P., Bopp, P. A., Limtrakul, J. (2009). Structure and dynamics of water confined in single-wall nanotubes. *Journal of Physical Chemistry A, 113*(10), 2103–8.
32. Zou, J., Ji, B. H., Feng, X. Q., Gao, H. J. (2006). Molecular-dynamic studies of carbon-water-carbon composite nanotubes. *Small, 2*(11), 1348–55.
33. Xu, J. Z., Chen, C., Wang, Y., Tang, H., Li, Z. M., Hsiao, B. S. (2011). Graphene nanosheets and shear flow induced crystallization in isotactic polypropylene nanocomposites. *Macromolecules, 44*(8), 2808–18.
34. Meng, J. S., Zhang, Y. Y., Cranford, S. W., Minus, M. L. (2014). Nanotube dispersion and polymer conformational confinement in a nanocomposite fiber: a joint computational experimental study. *Journal of Physical Chemistry B, 118*(31), 9476–85.
35. Xia, W., & Keten, S. (2015). Interfacial stiffening of polymer thin films under nanoconfinement. *Extreme Mechanics Letters, 4*, 89–95.
36. Qin, Z., Dimas, L., Adler, D., Bratzel, G., Buehler, M. J. (2014). Biological materials by design. *Journal of Physics-Condensed Matter, 26*(7), 073101.